Rational HIV Immunogen Design to Target Specific Germline B Cell Receptors

Joseph Jardine *et al.*
Science **340**, 711 (2013);
DOI: 10.1126/science.1234150

23. R. B. Cialdini, R. R. Reno, C. A. Kallgren, *J. Pers. Soc. Psychol.* **58**, 1015 (1990).
24. E. Krupka, R. A. Weber, *J. Econ. Psychol.* **30**, 307 (2009).
25. J. Sobel, *Markets and Other-Regarding Preferences* (Discussion Paper, Economics Department, Univ. of California, San Diego, 2010).
26. Median and modal prices in the bilateral market are 10 euros. Of all trades, 80.7% were in the range of 9 to 11 euros. In the multilateral market, all prices were below or equal to 10 euros, with one exception of a price of 10.1 euros.
27. The average price level in the bilateral market is 4.7 euros higher than in the multilateral market ($P < 0.0001$, $n = 468$, random fixed effects regression, with clustered standard errors on session level).
28. I. Kant, *Groundwork for the Metaphysics of Morals* (1785), L. Denis, Ed. (Broadview, Toronto, Canada, 2005), p. 93.
29. K. D. Vohs, N. L. Mead, M. R. Goode, *Science* **314**, 1154 (2006).
30. A. Kay, C. Wheeler, J. Bargh, L. Ross, *Organ. Behav. Hum. Decis. Process.* **95**, 83 (2004).
31. V. Liberman, S. M. Samuels, L. Ross, *Pers. Soc. Psychol. Bull.* **30**, 1175 (2004).
32. R. Frank, T. Gilovich, D. Regan, *J. Econ. Perspect.* **7**, 159 (1993).
33. A. E. Roth, *J. Econ. Perspect.* **21**, 37 (2007).
34. R. E. Lane, *The Market Experience* (Cambridge Univ. Press, Cambridge, 1991).
35. Charles-Louis de Montesquieu, Adam Smith, and Thomas Paine all expressed the view that markets and social behavior go hand in hand (*Doux-commerce Thesis*); see (*38*).
36. K. Arrow (*39*) points out that markets may require high levels of "professional ethics" (p. 36) to perform complex transactions under private information.
37. M. Spranca, E. Minsk, J. Baron, *J. Exp. Soc. Psychol.* **27**, 76 (1991).
38. A. Hirschman, *J. Econ. Lit.* **20**, 1463 (1982).
39. K. Arrow, *The Limits of Organization* (Norton, New York and London, 1974).

Rational HIV Immunogen Design to Target Specific Germline B Cell Receptors

Joseph Jardine,[1,2,3,4]* Jean-Philippe Julien,[2,3,5]* Sergey Menis,[1,2,3,4]* Takayuki Ota,[1] Oleksandr Kalyuzhniy,[1,2,3,4] Andrew McGuire,[6] Devin Sok,[1,2,3] Po-Ssu Huang,[4] Skye MacPherson,[1,2,3,4] Meaghan Jones,[1,2,4] Travis Nieusma,[2,3,5] John Mathison,[1] David Baker,[4] Andrew B. Ward,[2,3,5] Dennis R. Burton,[1,2,3,7] Leonidas Stamatatos,[6,8] David Nemazee,[1] Ian A. Wilson,[2,3,5,9] William R. Schief[1,2,3,4]†

Vaccine development to induce broadly neutralizing antibodies (bNAbs) against HIV-1 is a global health priority. Potent VRC01-class bNAbs against the CD4 binding site of HIV gp120 have been isolated from HIV-1–infected individuals; however, such bNAbs have not been induced by vaccination. Wild-type gp120 proteins lack detectable affinity for predicted germline precursors of VRC01-class bNAbs, making them poor immunogens to prime a VRC01-class response. We employed computation-guided, in vitro screening to engineer a germline-targeting gp120 outer domain immunogen that binds to multiple VRC01-class bNAbs and germline precursors, and elucidated germline binding crystallographically. When multimerized on nanoparticles, this immunogen (eOD-GT6) activates germline and mature VRC01-class B cells. Thus, eOD-GT6 nanoparticles have promise as a vaccine prime. In principle, germline-targeting strategies could be applied to other epitopes and pathogens.

Protection against disease by nearly all licensed vaccines is associated with induction of antibodies (*1*). Viruses with high antigenic diversity, such as HIV, influenza virus, and hepatitis C virus, pose major challenges for vaccine development (*2*). Most exposed surfaces on the Envelope glycoproteins (Env) of these viruses are hypervariable or shielded by glycans (*3*), and traditional vaccine approaches tend to induce neutralizing antibodies against only a small subset of viral strains (*4–6*). However, discoveries of bNAbs against each of these viruses have identified conserved epitopes as leads for vaccine design (*2*), and structural analysis has provided atomic definition for many of these epitopes (*7, 8*). Structure-based approaches are, therefore, needed to reverse-engineer vaccines capable of inducing bNAbs against these conserved epitopes (*9*).

High-potency VRC01-class bNAbs against the HIV gp120 CD4 binding site (CD4bs) have been isolated from several individuals infected with different strains of HIV-1 (*10–12*). VRC01-class bNAbs all derive from the human VH1-2*02 variable heavy gene but differ substantially in amino acid sequence and complementarity-determining region H3 (CDRH3) length and use a few different variable light chain genes (figs. S1 and S2). Structural studies have revealed that VRC01-class bNAbs employ a common mode of gp120 binding in which the VH1-2 framework mimics CD4 and provides additional electrostatic and hydrophobic contacts (Fig. 1A) (*12–15*). A short CDRL3 loop is also required for interaction with gp120 V5 and Loop D, and a CDRL1 deletion in many VRC01-class bNAbs avoids clashes with a glycan linked to Asn^{276} (N276) on loop D.

Vaccine design to induce VRC01-class bNAbs is attractive because VH1-2 genes are estimated to be present in ~2% of the human Ab repertoire (*16*) and, even considering restrictions on light chain usage, suitable precursors should be present in the naïve B cell repertoire of most individuals. However, predicted germline (GL) precursors for VRC01-class bNAbs exhibit no detectable affinity for wild-type Env (*11, 13*) (Table 1 and table S1), a potential explanation for the rarity of VRC01-class bNAbs in HIV-1 infection (*13*). More important, wild-type Env constructs lacking GL affinity are poor vaccine candidates to prime VRC01-class responses, because they are unlikely to reliably stimulate GL precursors to initiate antibody maturation.

Immunogen Design Strategy

To address the problem described above, we modified the CD4bs on a minimal, engineered outer domain (eOD) (*17*) to produce a germline-targeting vaccine prime (Fig. 1) with two important binding properties: (i) moderate affinity for multiple predicted VH1-2*02 GL-Abs to enhance the ability to activate VH1-2 GL B cells with appropriate light chains; (ii) high affinity for VRC01-class bNAbs to provide an affinity gradient to guide early somatic mutation toward

[1]Department of Immunology and Microbial Science, The Scripps Research Institute, La Jolla, CA 92037, USA. [2]International AIDS Vaccine Initiative Neutralizing Antibody Center, The Scripps Research Institute, La Jolla, CA 92037, USA. [3]Center for HIV/AIDS Vaccine Immunology and Immunogen Discovery, The Scripps Research Institute, La Jolla, CA 92037, USA. [4]Department of Biochemistry, University of Washington, Seattle, WA 98195, USA. [5]Department of Integrative Structural and Computational Biology, The Scripps Research Institute, La Jolla, CA 92037, USA. [6]Seattle Biomedical Research Institute, Seattle, WA 98109, USA. [7]Ragon Institute of Massachusetts General Hospital, Massachusetts Institute of Technology, and Harvard, Cambridge, MA 02129, USA. [8]Department of Global Health, University of Washington, Seattle, WA 98109, USA. [9]Skaggs Institute for Chemical Biology, The Scripps Research Institute, La Jolla, CA 92037, USA.

*These authors contributed equally to this work.
†Corresponding author. E-mail: schief@scripps.edu

the mature bNAbs. Furthermore, we developed self-assembling nanoparticles presenting 60 copies of the germline-targeting eOD to enhance B cell activation and to improve trafficking to lymph nodes (Fig. 1).

Engineering and Biophysical Analysis of Germline-Targeting Antigens

Modifications to the VRC01 epitope included removing clashes and building new contacts between the CD4bs and the GL-Abs, as well as rigidifying the CD4bs in a conformation that is favorable for binding. Initially, we constructed a homology model of GL-VRC01 bound to gp120 and identified a likely clash between CDRL1 and the N276 glycan. Therefore, we evaluated the GL-VRC01 binding of an eOD (eOD-Base) that lacks glycans at 276 and on the nearby V5 loop owing to N276D and N463D mutations. The eOD-Base barely interacted with GL-VRC01 ($K_D \sim 1$ mM) and had low affinity for only two of eight other GL VH1-2*02 Abs tested (Table 1). We then used Rosetta computational protein interface design (18) to identify other mutations in and around the CD4bs that were predicted to improve GL-VRC01 binding and created directed libraries that included all possible combinations of the computationally identified mutations. These libraries were screened for gp120 core and eOD variants that showed GL-VRC01 binding using yeast cell surface display (19). This strategy generated germline-targeting (GT) variants of gp120 core (CoreBal-GT1) and eOD (eOD-GT1) that bound GL-VRC01 with K_Ds of 1.8 µM and 44 µM, respectively (Table 1 and table S2). We focused further development on the smaller eOD because it lacks potentially distracting epitopes on gp120 core. A second round of computational design and directed-library screening produced eOD-GT2 with a three-fold improvement in K_D for GL-VRC01 (table S2). Subsequent screening of mixed computational/random mutagenesis libraries led to larger improvements and resulted in eOD-GT3 and eOD-GT4, which had K_Ds for GL-VRC01 of 220 and 34 nM, respectively (table S2). Interestingly, screening for GL-VRC01 binding also improved binding to other GL VH1-2 Abs, as eOD-GT4 bound to GL-NIH45-46 and GL-PGV19 with K_Ds of 1.0 µM and 28 nM, respectively (table S2). To achieve these improvements, eOD-GT4 had accumulated 17 mutations relative to eOD-Base.

To retain as native a CD4bs as possible (by reducing the number of mutations) while also maintaining or improving binding to GL VH1-2 Abs and mature bNAbs, we employed multi-target optimization. Here, libraries with either the wild-type HIV-1 strain HxB2 residue or the mutation in eOD-GT4 were sorted in parallel against multiple Abs, and mutations were retained only if they were positively selected by at least one GL Ab and not negatively selected by other Abs used during optimization. eOD-GT6 was generated by sorting against GL Abs for VRC01, NIH45-46, PGV19, PGV04, and VRC-CH31, as well as mature VRC01 and PGV04. eOD-GT6 had only eight mutations relative to eOD-Base (10 mutations relative to HxB2 gp120) and retained excellent binding to diverse GL VH1-2*02 Abs, with a K_D of 44 nM for GL-VRC01 and K_Ds < 500 nM for five of nine GL Abs tested (Table 1, table S2, and fig. S3). eOD-GT6 also had high affinity for several mature bNAbs, with K_Ds of 2, 4, and 88 nM for VRC01, NIH45-46, and PGV19, respectively, and maintained the desired affinity gradient for six of eight Abs tested (Table 1). Further, eOD-GT6 bound with high affinity to GL VRC01-class Abs derived from VH1-2*03 and *04 alleles (tables S3 and S4). eOD-GT6 had no detectable affinity for VH1-2*01, probably due to the absence of Trp[H50]; however, recent data from sequencing of 1092 human genomes (20) shows that the W50R mutation in VH1-2*01 occurs at a frequency of 0.21, indicating that only ~4% of the population are VH1-2*01 homozygotes not amenable to eOD-GT6 priming.

Crystallographic Analysis

To understand the molecular interaction of eOD-GT6 with GL-VRC01, we solved three crystal structures: unliganded GL-VRC01, unliganded eOD-GT6, and the complex of GL-VRC01 bound to eOD-GT6, to resolutions of 2.1 Å, 2.5 Å, and
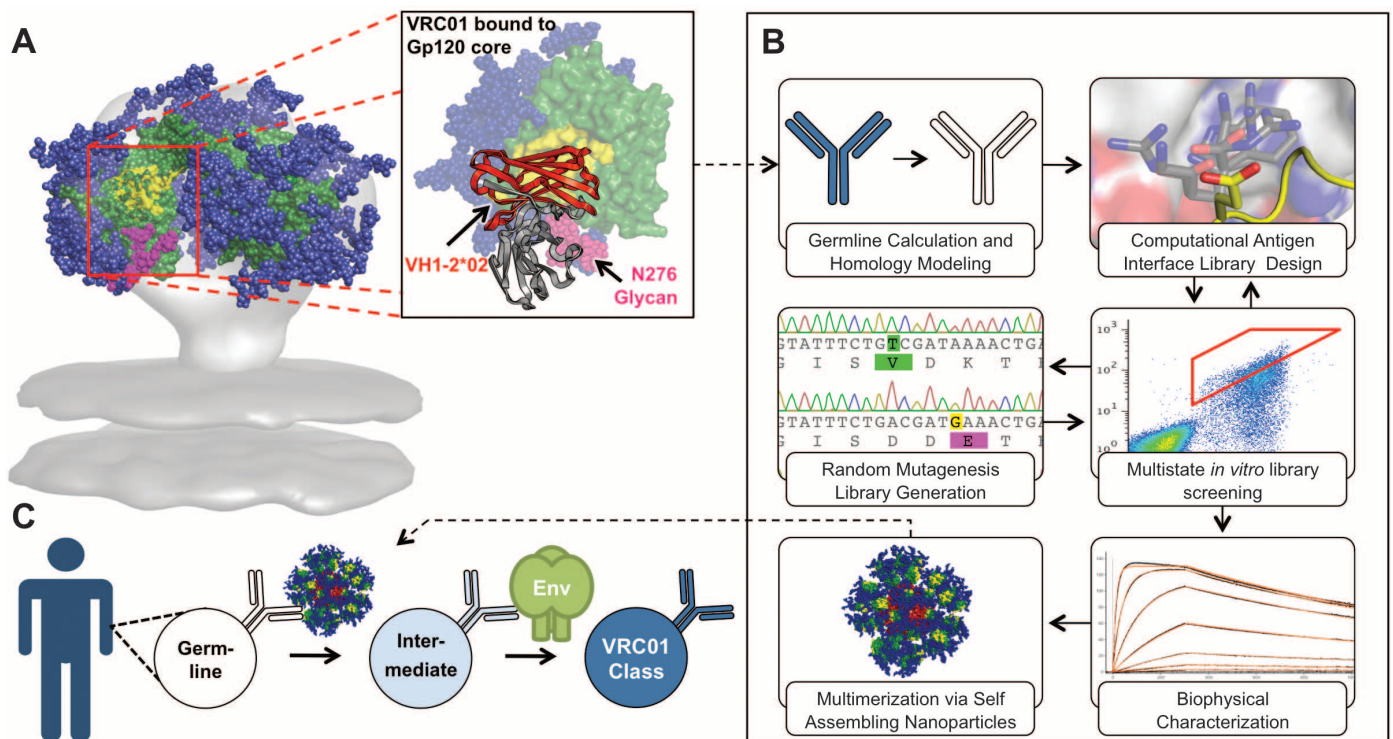
Fig. 1. Development of a germline (GL)–targeted HIV immunogen. (A) VRC01-class bNAbs bind to gp120 primarily through paratope residues encoded by VH 1-2*02. gp120 is colored green, with the CD4 binding site highlighted in yellow. Glycans are represented as blue spheres with the critical N276 highlighted in magenta. VRC01 is shown as a secondary structure rendering and colored gray, with the VH1-2*02 region highlighted in red. **(B)** Steps in the engineering of a modified gp120-based nanoparticle capable of activating GL VRC01-class B cells. **(C)** This nanoparticle can be used in an HIV-1 vaccine GL-prime-boost strategy to bridge this initial recognition gap and initiate clonal expansion and start somatic hypermutation of VRC01-class bNAbs precursors.

2.4 Å, respectively (Fig. 2 and table S4). The unliganded GL-VRC01 structure revealed that the gp120 contacting loops closely resemble those of VRC01 despite extensive affinity maturation of the latter (Fig. 2A and figs. S5 to S7). Unliganded eOD-GT6 showed a similar structure to the outer domains of unliganded and VRC01-bound gp120 core [1.2 Å Cα root mean square deviation (RMSD) in both instances] (Fig. 2B and fig. S8), suggesting good mimicry of the CD4bs. The structure of unliganded eOD-GT6 was also similar to eOD-GT6 bound to GL-VRC01 Fab (0.9 Å RMSD), with the largest differences occurring in the flexible loops and in the eOD exit loop (fig. S9). In addition, the structure of the eOD-GT6+GL-VRC01 complex indicated that the VH1-2–encoded domain of GL-VRC01 approaches eOD-GT6 at an angle nearly identical to that of VRC01 with gp120 (Fig. 2C) (4.2° angular difference when the complexes are superposed on the CD4 binding loop). Overall, the buried surface area (BSA) of GL-VRC01 (1076 Å²) on eOD-GT6 (1102 Å²) is nearly identical to VRC01 (1152 Å²) on gp120 core (1120 Å²), further demonstrating the high degree of similarity between the two structures (tables S5 and S6). Key hydrogen-bonding networks are preserved in the GL-VRC01+eOD-GT6 interaction, particularly in the CD4 binding loop (fig. S10). On the other hand, important differences in hydrogen bonds, BSA, and Cα positions are observed for interactions in loop D, V5, and the OD exit loop, which contribute to GL-VRC01 reactivity to eOD-GT6 (Fig. 2D and fig. S11).

Mutation Analysis

To understand the affinity contributions of individual mutations, we measured GL-VRC01 binding affinities for point reversions of each mutation (Table 2). Six mutations on eOD-GT6 conferred improved affinity for GL-Abs relative to the starting construct (eOD-Base) that lacked glycans at 276 and 463. The eOD-GT6+GL-VRC01 complex structure revealed that these mutations either are directly involved in the binding interface (T278R, I371F, and N460V) or stabilize loops involved in the interface (L260F, K357R, and G471S) (Fig. 2C). The two mutations with the largest effect on GL-VRC01 binding were G471S and I371F; reversion at these positions reduced GL-VRC01 affinity by factors of 39 and 10, re-

spectively (Table 2). Ser[471], together with Phe[371] and Phe[260], appear to play a role in altering the conformation of the OD exit loop to allow the GL-VRC01 CDRH2 to make H bonds with three additional gp120 residues (G472, G473, and D474) and bury an additional 120 Å² on gp120, resulting in improved binding (Fig. 2, C and D, right inset panel, tables S5 and S6, and fig. S9). Also, the N460V mutation located in V5 improves packing with the antibody and appears to contribute to an altered V5 conformation and pattern of V5 H-bonding with VRC01, as compared with Clade A/E 93TH057 gp120 recognition of VRC01 (Fig. 2D and fig. S12). Reversion of the N460V mutation reduced GL-VRC01 binding by a factor of 2.5 (Table 2).

Removal of key glycosylation sites was necessary for GL affinity. Reintroduction of the N276 glycosylation site in eOD-GT6 (by a double reversion, D276N/R278T) reduced binding by a factor of 140, and the remaining binding was likely due to a small fraction of the eOD-GT6-D276N/R278T that underutilized the N276 glycosylation position (fig. S13). Reversion of R278T alone reduced affinity by a factor of only 3.6 (Table 2). Thus, removal of the 276 glycan appears to release a block on GL-VRC01 binding but does not confer appreciable eOD affinity; further interface modification was required to achieve high affinity. Indeed, the eOD-GT6+GL-VRC01 complex structure revealed that, in addition to removing a clash between the N276 glycan and CDRL1 (Fig. 2C, left inset panel), eOD-GT6 D276 and R278 make two additional H-bonds with GL-VRC01. eOD-GT6 also lacks glycans at positions 386 (β12) and 463 (V5). Restoration of these glycosylation sites reduced affinity for GL-VRC01 by a factor of 3 (table S7).

eOD-GT6 Nanoparticle Generation

To enable eOD-GT6 to activate GL B cells via cross-linking of B cell receptors, and to develop a multivalent platform for eOD-GT6 that mimics the size, shape, multivalency, and symmetric surface geometry of many viruses for improved immunogenicity (21), we sought to fuse eOD-GT6 to a self-assembling virus-like nanoparticle. From a search of large homomeric particles in the Protein Data Bank (PDB), we prioritized 60-member of lumazine synthase from the hyperthermophile *Aquifex aeolicus* for experimental

testing due to their thermal stability and because modeling suggested that, with a suitable linker length, 60 copies of glycosylated eOD-GT6 could be sterically accommodated in an orientation that would expose the VRC01 epitope (Fig. 3A). Although expression of the wild-type particle had been reported in *Escherichia coli* (22), we found that such nanoparticles presenting glycosylated eOD-GT6 could be secreted from mammalian (293) cells and purified by lectin chromatography with good yield (~10 mg/L) and structural homogeneity (Fig. 3B and figs S14 and S15).

In Vitro B Cell Activation

The ability of eOD-GT6 nanoparticles to activate B cells expressing GL and mature VRC01 [immunoglobulin M (IgM)] (23), 12A12 (IgM and IgG), and NIH45-46 (IgG) (24) was tested in Ca²⁺-dependent activation assays. The nanoparticles potently activated both GL and mature B cells with 1 μM outer domain (16 nM particle) and modestly activated all three cell lines at 1000-fold lower concentrations (Fig. 3C and fig. S16). In contrast, monomeric eOD-GT6 was non-stimulatory, probably due to an inability to cross-link B cell receptors (23). Trimeric eOD-GT6 activated both GL and mature B cells, but less potently and rapidly than the 60-member nanoparticles, and a soluble gp140 trimer from HIV-1 strain YU2 (25) showed no activation of GL B cells but did activate the mature counterparts (Fig. 3C). Both IgM and IgG B cell lines were generated for GL 12A12, and we observed no significant differences in activation magnitude or kinetics between the two antibody isotypes (fig. S16).

Animal Models for Human VH1-2 Germline Targeting

We then assessed whether eOD-GT6 might interact with related GL-Abs in animal models. Analysis of VH genes from rabbit (fig. S17) (26), mouse (figs. S18 and S19) (27), and macaque (fig. S20) revealed that none of these commonly used model organisms have a known VH gene containing all of the critical residues for GL binding (15). To measure binding experimentally, chimeric GL-Abs were produced in which the human VH1-2*02 gene from GL-VRC01 was replaced with GL VH genes from mice or macaques containing the essential Arg[H71] and as many other

Table 1. Binding of GL and mature (Mat) antibodies to gp120 and eOD variants. Values represent K_Ds in nM measured by surface plasmon resonance (SPR). Detectable binding to GL antibodies is in boldface.

Antigen		Antibody														
		VRC01		12A12		3BNC60		NIH45-46		PGV04		PGV19		PGV20		VRC-CH31	
		GL	Mat	GL	Mat	GL	Mat	GL	Mat	GL	Mat	GL	Mat	GL	Mat	GL	Mat
Wild-type	Core.HXB2	>10⁵	5	>10⁵	6	>10⁵	36	>10⁵	35	>10⁵	48	>10⁵	20	>10⁵	19	>10⁵	47
Germline-targeted	eOD-Base N276D	>10⁵	5	>10⁵	380	>10⁵	4100	>10⁵	14	>10⁵	110	>10⁵	3100	**17,000**	16	>10⁵	30,000
	Core.BaL-GT1	**1800**	0.5	**3200**	1	**16,400**	4	>10⁵	0.6	>10⁵	170	**25**	14	**5,500**	4	**35,000**	1800
	eOD-GT1	**44,000**	1	>10⁵	2300	>10⁵	83	>10⁵	3	>10⁵	4	**7800**	1000	**1100**	10	>10⁵	>10⁵
	eOD-GT6	**44**	2	**2000**	400	**14,000**	200	**410**	4	52,000	10	**19**	88	**3**	6	**28,000**	29,000

Fig. 2. Structural analysis of GL-VRC01 and eOD-GT6. (**A**) The structure of the unliganded inferred GL-VRC01 antibody (heavy and light chains colored blue and yellow, respectively) is similar to the structure of gp120-bound VRC01 (white) within the gp120-contacting positions (shown in orange on VRC01, defined by the structure of VRC01+gp120 in PDBID:3NGB). Structures are rendered according to B values, with thin and thick lines representing areas possessing low and high flexibility, respectively. (**B**) Comparison between the crystal structures of unliganded eOD-GT6 (green) and unliganded gp120 core from HIV-1 strain 93TH057 (PDBID: 3TGT, white). Structures rendered as in (A). (**C**) Comparison between the crystal structures of GL-VRC01+eOD-GT6 and VRC01+gp120 core (PDBID: 3NGB), in which only the outer domain of gp120 is shown. Structures rendered as in (A) and (B), except gp120-contacting positions on VRC01 are white. The mutated residues in eOD-GT6 that enable binding of GL-VRC01-class Abs are shown as space-fill magenta spheres. The angle of approach of GL-VRC01 and VRC01 to the CD4bs is nearly identical. Key regions where interactions are different between VRC01 on gp120 (upper panels) and GL-VRC01 on eOD-GT6 (lower panels) are shown in insets. eOD-GT6 confers germline reactivity by removing a potential clash with the N276 glycan, as well as by creating additional contacts with loop D (left panels), the OD exit loop (right panels) and V5 (fig. S12). (**D**) gp120 residues involved in the VRC01+gp120 and GL-VRC01+eOD-GT6 interfaces are compared in sequence, hydrogen bonding (stars), buried surface area, and RMSD. Interfaces were calculated using PDBePISA (29) and Cα RMSD using Chimera (30). Single-letter abbreviations for the amino acid residues are as follows: A, Ala; C, Cys; D, Asp; E, Glu; F, Phe; G, Gly; H, His; I, Ile; K, Lys; L, Leu; M, Met; N, Asn; P, Pro; Q, Gln; R, Arg; S, Ser; T, Thr; V, Val; W, Trp; and Y, Tyr.

critical residues as possible. Chimeric GL-Abs with mouse VH genes had no detectable binding to eOD-GT6. Chimeric Abs derived from two of the three rhesus VH genes bound weakly to eOD-GT6, with K_Ds of ~30 μM and ~40 μM (table S8). The rhesus chimeric GL-Ab most similar to human GL-VRC01 contained only 10 mutations in the VH gene (95.5% identity over the antibody Fv region) but showed no detectable binding to eOD-GT6. Annotation of the rhesus macaque antibody repertoire and analysis of gene usage frequencies will be useful to construct bona fide macaque GL VH1-2 Abs. These

analyses illustrate the potential difficulty for using animal models to produce VRC01-class bNAbs and suggest that immunization of humans or mice engineered to produce human Abs may be essential for testing and iteratively optimizing such immunogens.

Concluding Remarks
The events that led to GL VH1-2*02 B cell activation in the HIV-infected individuals from which VRC01-class bNAbs were isolated remain unclear. Our finding that a small number of rare or previously undocumented Env mutations con-

fers high affinity GL binding suggests that Env variants might have acquired one or more such mutations stochastically during infection and thereby gained the ability to prime GL VRC01-class B cells. Vaccines to induce VRC01-class responses will need to activate such B cells dependably and drive appropriate somatic mutation to produce high-affinity bNAbs (28). We propose the eOD-GT6 nanoparticle as a promising candidate for a vaccine prime based on its ability to bind diverse VH1-2*02 GL Abs, activate VRC01, 12A12, and NIH45-46 B cell lines in vitro, and provide an affinity gradient for early

Table 2. Binding of GL VRC01 to eOD-GT6 point reversions. Values represent K_Ds in nM measured by SPR. Amino acid frequencies determined from 2867 HIV-1 sequences from www.hiv.lanl.gov. epPCR, error-prone polymerase chain reaction.

	eOD-GT6	Single reversions					
Reversion from eOD-GT6	–	F260L	R278T	R357K	F371I	V460N	S471G
Frequency of WT amino acids	–	L (97.3%)	T (78.4%)	K (68.9%)	I (85.8%)	N (36.2%)	G (78,7%)
Frequency of mutation	–	F (0.0%)	R (0.1%)	R (0.5%)	F (0.0%)	V (3.4%)	S (0.5%)
Method of discovery	–	epPCR	Rosetta	epPCR	Rosetta	Rosetta	epPCR
GL-VRC01 affinity (nM)	44	310	160	64	450	120	1,700
Change from eOD-GT6	–	7.0	3.6	1.5	10.3	2.7	39
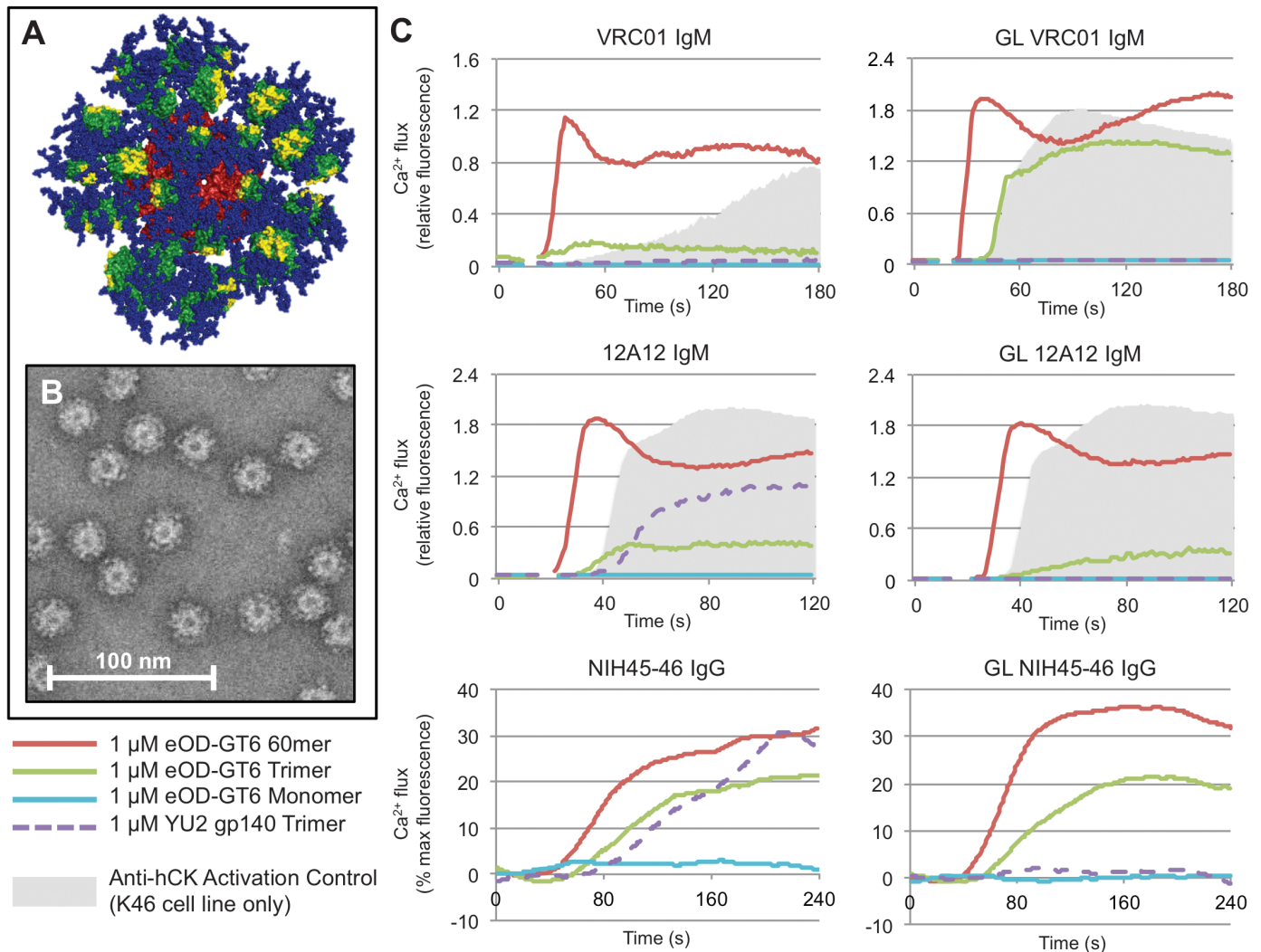
Fig. 3. A 60-member eOD-GT6 nanoparticle activates GL and mature VRC01-class B cells. (**A**) Model representation of the 60-member eOD-GT6 nanoparticle. eOD-GT6 is colored in green, with residues that interact with VRC01 colored in yellow. Glycans are shown as blue spheres, and the self-assembling 60-member lumazine synthase to which eOD-GT6 is fused is colored red. (**B**) Raw negative stain electron microscopy image of the 60-member eOD-GT6 nanoparticle. (**C**) Calcium flux experiments show that the 60-member eOD-GT6 nanoparticle activates B cell lines engineered to express either GL or mature VRC01 IgM, 12A12 IgM, or NIH45-46 IgG, whereas a recombinant soluble gp140 trimer activates the B cells expressing mature, but not GL VRC01-class, antibodies. Data for each antibody are representative of at least two separate experiments.

somatic mutation. We further propose that ultimate elicitation of mature VRC01-class bNAbs will require, at minimum, boosting with different immunogens that present a less engineered, more native CD4bs, including the glycans around the CD4bs.

References and Notes
1. S. A. Plotkin, *Clin. Vaccine Immunol.* **17**, 1055 (2010).
2. D. R. Burton, P. Poignard, R. L. Stanfield, I. A. Wilson, *Science* **337**, 183 (2012).
3. W. R. Schief, Y.-E. A. Ban, L. Stamatatos, *Curr. Opin. HIV AIDS* **4**, 431 (2009).
4. D. R. Burton et al., *Cell Host Microbe* **12**, 396 (2012).
5. D. C. Ekiert et al., *Science* **324**, 246 (2009).
6. P. Zhang et al., *Proc. Natl. Acad. Sci. U.S.A.* **106**, 7537 (2009).
7. J. P. Julien, P. S. Lee, I. A. Wilson, *Immunol. Rev.* **250**, 180 (2012).

8. L. Kong et al., Proc. Natl. Acad. Sci. U.S.A. **109**, 9499 (2012).
9. D. R. Burton, Nat. Rev. Immunol. **2**, 706 (2002).
10. X. L. Wu et al., Science **329**, 856 (2010).
11. J. F. Scheid et al., Science **333**, 1633 (2011).
12. X. Wu et al.; NISC Comparative Sequencing Program, Science **333**, 1593 (2011).
13. T. Q. Zhou et al., Science **329**, 811 (2010).
14. R. Diskin et al., Science **334**, 1289 (2011).
15. A. P. West Jr., R. Diskin, M. C. Nussenzweig, P. J. Bjorkman, Proc. Natl. Acad. Sci. U.S.A. **109**, E2083 (2012).
16. R. Arnaout et al., PLoS ONE **6**, e22365 (2011).
17. R. Pejchal et al., Science **334**, 1097 (2011).
18. A. Leaver-Fay et al., Methods Enzymol. **487**, 545 (2011).
19. G. Chao et al., Nat. Protoc. **1**, 755 (2006).
20. G. R. Abecasis et al.; 1000 Genomes Project Consortium, Nature **491**, 56 (2012).
21. M. F. Bachmann, G. T. Jennings, Nat. Rev. Immunol. **10**, 787 (2010).
22. X. Zhang, W. Meining, M. Fischer, A. Bacher, R. Ladenstein, J. Mol. Biol. **306**, 1099 (2001).
23. T. Ota et al., J. Immunol. **189**, 4816 (2012).
24. S. Hoot et al., PLoS Pathog. **9**, e1003106 (2013).
25. C. Sundling et al., J. Exp. Med. **207**, 2003 (2010).
26. K. L. Knight, C. R. Winstead, Curr. Opin. Immunol. **9**, 228 (1997).
27. Several mouse VH genes were identified that contained the Arg[H71] important for eOD-GT6 binding, but crystal structures of mouse Abs indicated that Arg[H71] would not be accessible for binding because it forms internal H bonds with backbone carbonyl groups (fig. S19).
28. B. F. Haynes, G. Kelsoe, S. C. Harrison, T. B. Kepler, Nat. Biotechnol. **30**, 423 (2012).
29. E. Krissinel, K. Henrick, J. Mol. Biol. **372**, 774 (2007).
30. E. F. Pettersen et al., J. Comput. Chem. **25**, 1605 (2004).

REPORTS

Lorentz Meets Fano in Spectral Line Shapes: A Universal Phase and Its Laser Control

Christian Ott,[1] Andreas Kaldun,[1] Philipp Raith,[1] Kristina Meyer,[1] Martin Laux,[1] Jörg Evers,[1] Christoph H. Keitel,[1] Chris H. Greene,[3] Thomas Pfeifer[1,2]*

Symmetric Lorentzian and asymmetric Fano line shapes are fundamental spectroscopic signatures that quantify the structural and dynamical properties of nuclei, atoms, molecules, and solids. This study introduces a universal temporal-phase formalism, mapping the Fano asymmetry parameter q to a phase φ of the time-dependent dipole response function. The formalism is confirmed experimentally by laser-transforming Fano absorption lines of autoionizing helium into Lorentzian lines after attosecond-pulsed excitation. We also demonstrate the inverse, the transformation of a naturally Lorentzian line into a Fano profile. A further application of this formalism uses quantum-phase control to amplify extreme-ultraviolet light resonantly interacting with He atoms. The quantum phase of excited states and its response to interactions can thus be extracted from line-shape analysis, with applications in many branches of spectroscopy.

I
n spectroscopic detection of electromagnetic radiation, the sample's temporal dipole response—the time-dependent dipole moment of the system after an infinitesimally short (Dirac delta function) excitation—gives rise to line shapes observed in fluorescence or absorption. If a continuum of states is excited, this temporal dipole response corresponds also to a delta function, which is the superposition of a continuous spectrum of emitting dipoles at all frequencies. The more commonly observed exponential decay of a discrete excited state with a finite lifetime gives rise to the well-known symmetric Lorentzian line shape.

Asymmetric Fano absorption line shapes emerge when discrete excited states are coupled to a continuum of states (1, 2), which is a general phenomenon throughout nuclear (3), atomic (4–6), and solid-state physics (7–10), as well as molecular spectroscopy in chemistry (11). As a result of this discrete-continuum coupling mech-anism, the temporal dipole response function is not just the sum of the exponentially decaying and deltalike dipole responses of the isolated state and continuum, respectively. The exponential dipole response is shifted in phase with respect to the Lorentzian response, which is the origin of the asymmetric line shape of the Fano resonance. By a mathematical transformation [supplementary text (12) section 1] similar to the one recently conducted for a classical Fano oscillator (13), we mapped this phase shift φ in the time domain into the q parameter, which was introduced by Ugo Fano (1, 2) and thereafter used to characterize and quantify the asymmetric Fano line shape. The cross section at photon energy $E = \hbar\omega$ is given in terms of q by

$$\sigma_{Fano}(E) = \sigma_0 \frac{(q+\varepsilon)^2}{1+\varepsilon^2}, \varepsilon = \frac{E-E_0}{\hbar(\Gamma/2)} \quad (1)$$

where ε denotes the reduced energy containing E_0 and Γ as the position and width of the resonance, respectively, $\hbar$ denotes the reduced Planck constant, and σ_0 is the cross section far away from the resonance.

In general, the absorption cross section σ_{abs} is proportional to the imaginary part of the index of refraction, which in turn is directly related to the polarizability (5) and thus to the frequency-dependent dipole response function $d(E)$:

$$\sigma_{abs}(E) \propto Im[d(E)] \quad (2)$$

Via the Fourier transform, $d(E)$ is connected to the time-dependent linear response $\tilde{d}(t)$ of the medium after a deltalike excitation pulse. For a Lorentzian spectral line shape of width Γ, $\tilde{d}_{Lorentz}(t)$ is an exponentially decaying function

[1]Max-Planck-Institut für Kernphysik, 69117 Heidelberg, Germany. [2]Center for Quantum Dynamics, Ruprecht-Karls-Universität Heidelberg, 69120 Heidelberg, Germany. [3]Department of Physics, Purdue University, West Lafayette, IN 47907, USA.

*Corresponding author. E-mail: thomas.pfeifer@mpi-hd.mpg.de